Theoretical Structure and Vibrational Analysis of Ethyl Methanesulfonate, $CH_3SO_2OCH_2CH_3$

M. E. Tuttolomondo,[†] A. Navarro,*[,‡] T. Peña,[‡] E. L. Varetti,[§,||] and A. Ben Altabef [†,||]

Instituto de Química Física, Facultad de Bioquímica, Química y Farmacia, Universidad Nacional de Tucumán, San Lorenzo 456, 4000 Tucumán, Argentina, Departamento de Química Física y Analítica, Universidad de Jaén, Campus Las Lagunillas, 23071 Jaén, Spain, and Centro de Química Inorgánica and Laboratorio Nacional de Investigación y Servicios en Espectrofotometría Óptica (CEQUINOR and LANAIS EFO, CONICET-UNLP), Departamento de Química, Facultad de Ciencias Exactas, Universidad Nacional de La Plata, C. Correo 962, 1900 La Plata, Argentina

Received: February 25, 2005; In Final Form: July 12, 2005

Ethyl methanesulfonate, $CH_3SO_2OCH_2CH_3$, is well-known as an alkylating agent in mutagenic and carcinogenic processes. Its electronic structure and that of the methanesulfonate anion ($CH_3SO_3^-$) were determined using optimization methods based on density functional theory and Moller−Plesset second-order perturbation theory. For $CH_3SO_2OCH_2CH_3$, two conformations with symmetries C_s and C_1 are obtained, the former being more stable than the latter. Natural bond orbital (NBO) calculations show the C_s conformation provides a more favorable geometry of the lone pairs of the oxygen atom linking the ethyl group. The NBO technique also reveals the characteristics of the methanesulfonate anion as a leaving group due to the rearrangement of the excess electronic charge after alkylation. Furthermore, the infrared spectra of $CH_3SO_2OCH_2CH_3$ are reported for the liquid and solid states as well as the Raman spectrum of the liquid. Comparison to experiment of the conformationally averaged IR spectrum of C_s and C_1 provides evidence of the predicted conformations in the solid IR spectrum. These experimental data along with the calculated theoretical force constants are used to define a scaled quantum mechanical force field for the target molecule, which allowed the measured frequencies to be reproduced with a final root-mean-square deviation of 9 cm^{-1} and, thus, a reliable assignment of the vibrational spectrum.

1. Introduction

Ethyl methanesulfonate (EMS) is a monofunctional ethylating agent which has been the subject of detailed analyses for a number of years. From the first studies in 1960s until the present, thousands of papers have been published dealing with the mutagenic effects in a wide variety of genetics systems from viruses to mammals, also showing the carcinogenic effects in the latter.[1] Recently, its determination in pharmaceutical products have been studied by capillary gas chromatography.[2] Furthermore, it has been shown that alkylation of cellular nucleophilic sites by EMS occurs by mixed SN1 (unimolecular) and SN2 (bimolecular) nucleophilic substitution mechanisms.[3] The leaving group is the weak conjugate base named the mesylate anion, $CH_3SO_2O^-$, which can easily accept and stabilize electron charge after nucleophilic attack, an essential requirement for a good leaving group.

Despite the wide field of applications of this system, neither molecular structure nor vibrational characteristics of EMS and the mesylate anion have been studied so far. The purpose of the present work is to obtain a first approximation to the molecular structure of EMS and mesylate anion by performing quantum mechanical calculations in order to describe, from a theoretical point of view, the electronic properties of the parent system as a potent mutagenic and carcinogenic agent in biomedical research. To achieve this, the fully optimized geometry was obtained for $CH_3SO_2OCH_2CH_3$ using density functional theory (B3LYP) in combination with standard split-valence basis sets 6-31G*, 6-311G**, and 6-311++G**, Moller−Plesset second-order perturbation theory (MP2) implementing the 6-31G* basis set, and the more recent hybrid functionals PBE1PBE and MPW1PW91 in combination with the 6-311++G** basis set. The mesylate anion structure was also optimized using UB3LYP/6-311++G**, UMP2/6-31G*, UPBE1PBE/6-311++G**, and UMPW1PW91/6-311++G** methods. Natural bond orbital (NBO)[4] calculations at the B3LYP/6-311++G** and UB3LYP/6-311++G** levels have been carried out for both the EMS and mesylate anion, respectively, to explain the relative stabilization of the C_s conformer with respect to C_1 in the former species and the electron charge stabilization in the latter. It is of great interest to compare the molecular geometric parameters and conformations with those for similar compounds, some of them already studied, such as $CF_3SO_2OCH_3$,[5] $CF_3SO_2OSiH_3$,[6] $CF_3SO_2OSi(CH_3)_3$,[7] $CF_3SO_2OCH_2CF_3$,[8] $CCl_3SO_2OCH_2CF_3$,[9] $CF_3SO_2OCH_2CH_3$,[10] and $CH_3SO_2OCH_3$.[11]

Furthermore, the first vibrational analysis is reported measuring the IR and Raman spectra for EMS. The spectral features were subsequently assigned to the different normal modes of vibration, and the scaled force field was obtained by following Pulay's methodology.[12−15]

* Corresponding author. Tel: +34−953-212756. Fax: 34−953-212141. E-mail: anavarro@ujaen.es.
[†] Universidad Nacional de Tucumán.
[‡] Universidad de Jaén.
[§] Universidad Nacional de La Plata.
[||] Members of the Carrera del Investigador Científico, CONICET, R. Argentina.

10.1021/jp0509865 CCC: $30.25
Published on Web 08/16/2005

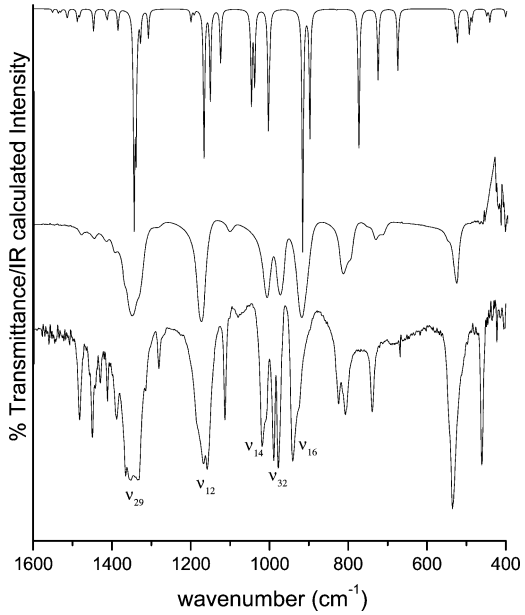

Figure 1. Calculated (top) and experimental infrared spectra (middle, liquid; bottom, solid) of $CH_3SO_2OCH_2CH_3$ between 400 and 1600 cm^{-1}. The calculated spectrum was obtained from B3LYP/6-31G* frequencies and intensities using Lorentzian band shapes and populations for both conformers.

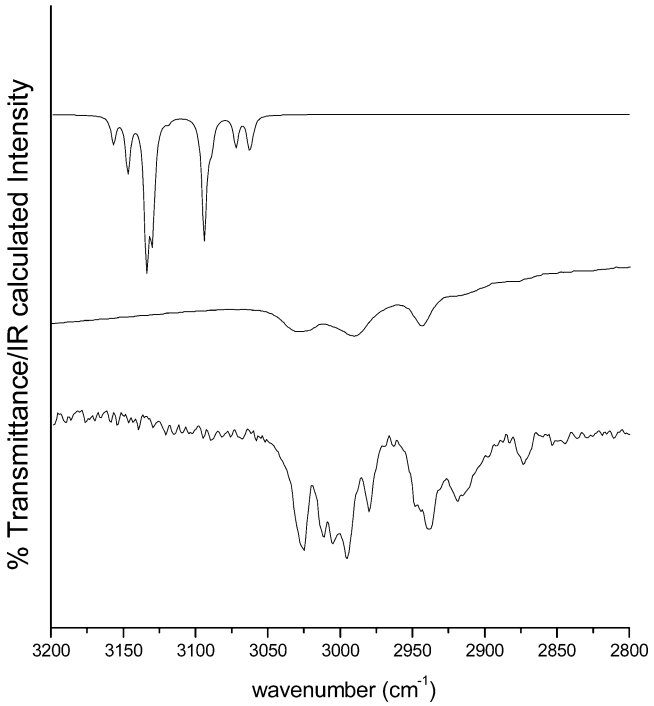

Figure 2. Calculated (top) and experimental infrared spectra (middle, liquid; bottom, solid) of $CH_3SO_2OCH_2CH_3$ between 2800 and 3200 cm^{-1}. The calculated spectrum was obtained from B3LYP/6-31G* frequencies and intensities using Lorentzian band shapes and populations for both conformers.

2. Experimental Section

$CH_3SO_2OCH_2CH_3$ (Aldrich Products, Inc.) was used with no further purification and handled with proper protection from the atmospheric humidity. The safety requirements of glasses, gloves, and good ventilation were respected when handling the sample because of its carcinogenic properties. Spectra were obtained using a Perkin-Elmer 1760-X FTIR instrument and in a FT-Raman RFS 100/S with a Nd:YAG laser emitting at 1064 nm (laser power 500 mW) and a liquid N_2 cooled Ge detector. An IR spectrum of the substance maintained as a film between KBr windows and frozen at about 197 K was run in a variable temperature RIIC (VLT-2) cell, using a Perkin-Elmer FTIR instrument, model 1600, in order to obtain better definition of some bands. The spectral resolution was 1 cm^{-1} in all the cases.

Representative spectra are illustrated in Figures 1 and 2 (IR spectra of the liquid and solid) and 3 (Raman spectrum of the liquid), and the frequencies of the observed spectral features are collected in Table 1.

TABLE 1: Frequencies of Observed Bands in the Infrared and Raman Spectra of $CH_3SO_2OCH_2CH_3$ (units are cm^{-1})

IR[a]			
liquid	solid	Raman liquid[b]	assignment
	3031 sh		ν_{24}
3027 w, br	3027 w	3025 (20)	ν_1
	3013		ν_{25}
	3006 vw		?
2989 w	2996 w	2990 (24)	ν_2
	2981 w		ν_{26}
	2947 sh		ν_3
2943 w		2942 (100)	
	2939 w		ν_4
2918	2918 w		?
2875	2874	2878	ν_5
1479 w	1482 m		ν_6
1460 sh	1457	1458(7)	ν_7
1447 w	1450 m	1447 (6)	ν_{27}
	1430 w		ν_{28}
1416 w		1417 (1)	
	1411 w		ν_8
1394 w	1389 w		ν_9
1368 sh	1365		?
1351 vs	1352 vs	1353 (6)	ν_{29}
	1328 vs		ν_{11}
1288 sh	1281 w	1283 (3)	ν_{30}
1175 vs	1169 vs		ν_{12}
	1158 vs		
		1168 (28)	ν_{31}
1103 w	1113 m	1102 (10)	ν_{13}
1009 m	1018 s	1008 (4)	ν_{14}
	1011 sh		
	989 s		ν_{15}
976 m		975 br	
	977 s		ν_{32}
921 s			ν_{16}
	940 s		
	927 sh		
816 m	825 m		ν_{17}
797 sh	807 m	798 (4)	ν_{33}
733 w	740 m	735 (23)	ν_{18}
717 w		717 sh	?
550 vw		550 (3)	ν_{19}
530 m	535 m	530 (14)	ν_{20}
463 w	461 m	463(7)	ν_{34}
358 sh		358 sh	ν_{21}
338 w		339 (12)	ν_{22}
325 sh		ca. 321 sh	ν_{35}
287 vw		287	ν_{36}
227 vw			ν_{37}
		200 br	ν_{23}
		85 (6)	ν_{38}

[a] sh,shoulder; br, broad; s, strong; w, weak; m, medium; v, very. [b] Relative band heights in parentheses.

3. Computational Details

Fully optimized geometries were obtained for ethyl methanesulfonate, $CH_3SO_2OCH_2CH_3$, and the mesylate anion, $CH_3SO_3^-$, using DFT with the B3LYP[16,17] hybrid functional in combination with the standard split-valence basis sets 6-31G*, 6-311G**,

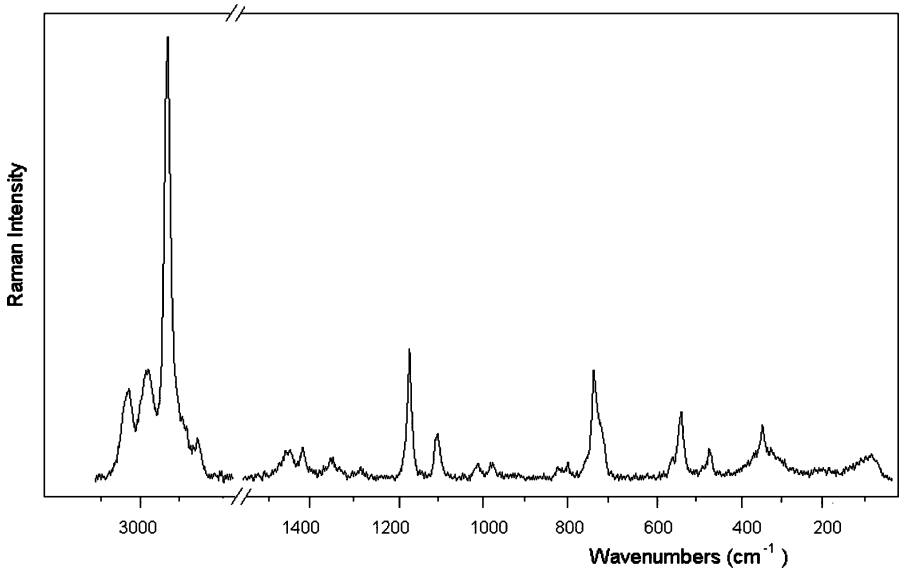

Figure 3. Normal Raman spectrum of liquid $CH_3SO_2OCH_2CH_3$ between 3200 and 60 cm^{-1}.

and 6-311++G**.[18] In addition, MP2/6-31G*,[18] PBE1PBE/6-311++G**, [19] and MPW1PW91/6-311++G** [20] were used. For the anion, unrestricted calculations by using MP2/6-31G* and DFT methods with the B3LYP, PBE1PBE, and MPW1PW91 functionals were performed, and only the 6-311++G** basis set was used. Vibrational frequencies and force constants were calculated from analytic first and second derivatives of the potential energy. All the calculations were performed using the Gaussian 98 package of programs.[21] The natural bond orbital (NBO) calculation was performed at the B3LYP/6-311++G** and UB3LYP/6-311++G** for the EMS and mesylate anion, respectively, using the program NBO 4.0 code as implemented in the Gaussian 98 package.[22]

The harmonic force field in Cartesian coordinates for $CH_3SO_2OCH_2CH_3$ which resulted from the DFT procedure was transformed to a set of natural (local symmetry) coordinates through the B matrix[23] obtained with a standard program. The resulting force field was subsequently scaled using the scheme of Pulay et al.[12−15] in which the diagonal force constants are multiplied by scale factors f_i , f_j, ..., and the corresponding interaction constants are multiplied by $(f_i. f_j)^{1/2}$. The scale factors were refined to fit the experimental frequencies. All the vibrational bands were assigned the same weight in the refinement except those missing or showing uncertain frequencies where the zero value was used. No empirical correction of the theoretical geometry was used. The potential energy distribution was subsequently calculated with the resulting scaled quantum mechanics (SQM) force field.

The force field transformation, scaling, and potential energy distribution calculations were performed with the program FCARTP.[24] The atomic displacements given by the Gaussian 98 code for each vibrational mode served to understand qualitatively the nature of the molecular vibrations; for that purpose, the corresponding data were represented graphically by means of the program GaussView.[25]

4. Structural Results

No theoretical or experimental structure data are available either for the $CH_3SO_2OCH_2CH_3$ molecule or for the $CH_3SO_3^-$ anion, and therefore the first goal of the present work was to obtain the most stable molecular conformation. For the EMS, different relative orientations for the SCH_3 and CCH_3 groups as well as the C−S−O−C and S−O−C−C torsion angles were used. For this purpose, we defined six initial conformations, keeping a pseudotetrahedral hybridization for the C_1, S_5, O_8, C_9, and C_{10} in all of them (see Figure 4). These starting structures were generated by using the program GaussView.[25] The geometries of these conformers were optimized at the B3LYP/6-31G* level without any symmetry constraints until the default convergence criteria were satisfied. As a result, two different conformations were obtained: one of them, named as I, with C_1 symmetry and a more stable one, named as II, with C_s symmetry. To confirm the secondary minimum, two series of calculations in which the molecular geometry was optimized for fixed values of either the CSOC or the SOCC dihedral angles were performed, in 10° steps. Due to computational limitations, the HF/6-31G* approximation was used in these calculations. The results are shown in Figures 5 and 6, where conformations I and III are equivalent.

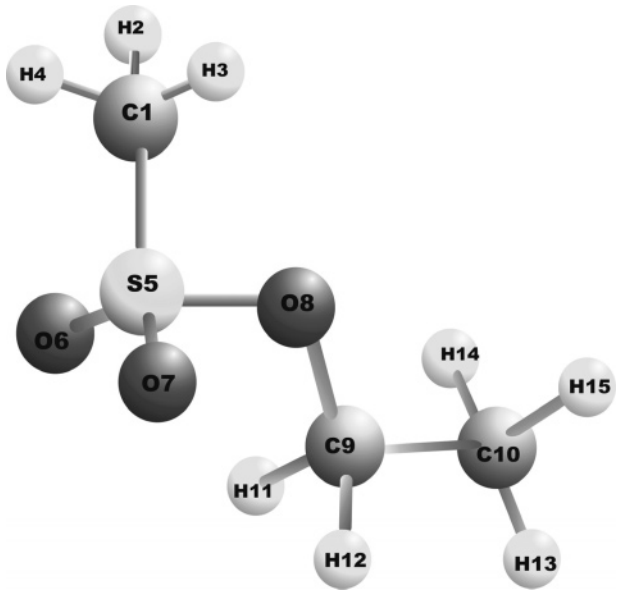

Figure 4. Atom numbering and definition of internal coordinates for $CH_3SO_2OCH_2CH_3$. Definition of angles: φ, O_8-C_9-H; λ, $C_{10}-C_9-H$; z, $H-C_9-H$; ϵ, $H-C_1-H$; π, $H-C_{10}-H$; β, $H-C_1-S$; μ, $H-C_{10}-H$; α, $S-O-C_9$; x, O−C−C; θ, C_1-S-O; ψ, C−S═O; γ, O−S═O; ϕ, O═S═O. Definition of torsions: τ(S−O), $C_1-S-O-C_9$; τ(C−O), S−O−C−C; $\tau(SCH_3)$, $O-S-C_1-H_j$; $\tau(CCH_3)$, $O-C_9-C_{10}-H_i$.

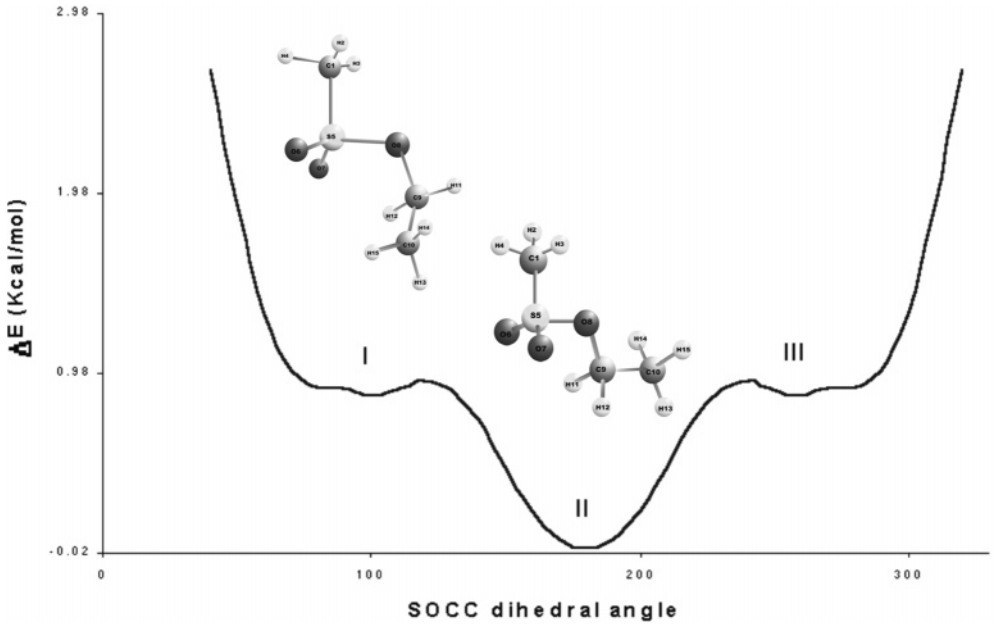

Figure 5. Relative energy of the $CH_3SO_2OCH_2CH_3$ molecule as a function of the SOCC dihedral angle and final conformations.

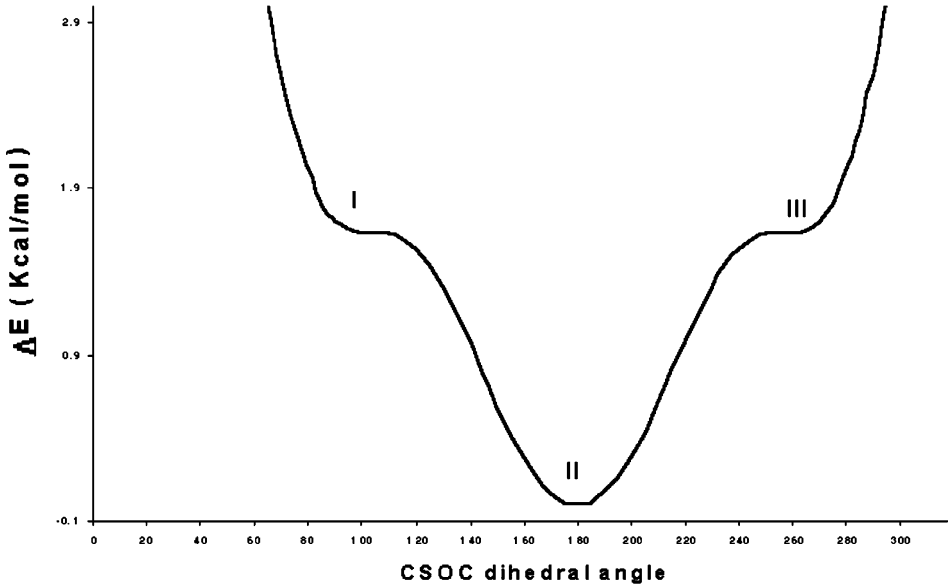

Figure 6. Relative energy of the $CH_3SO_2OCH_2CH_3$ molecule as a function of the CSOC dihedral angle and final conformations.

To test the dependence between the results for the most stable conformation and method used, further geometry optimizations for the EMS by using B3LYP together with 6-311G** and 6-311++G** basis sets, MP2/6-31G*, PBE1PBE/6-311++G**, and MPW1PW91/6-311++G** methods were used. The structural results obtained in these calculations are reported in Table 2 and the molecular energy for the minima in Table 3. No correction for zero point energy (ZPE) was made.

The comparison of MP2 and DFT data yields differences that vary by 0.02 Å for the C1−S5 bond when using the B3LYP functional, while for PBE1PBE and MPW1PW91 they decrease to 0.001−0.003 Å. For S═O, S−O, and O−C bonds, the trend is reversed. For the remaining distances, the differences are always less than 0.02 Å, and for the bond angles, the highest variation when comparing MP2 and DFT methods is 2.7° (B3LYP/6-311++G**) for S5−O8−C9.

For the B3LYP functional, the differences in bond distances, when increasing the size of the basis set, are shorter than 0.01 Å, while for the bond angles, the highest differences are found for S5−O8−C9 showing values up to 1.3° with the remaining bond angles being shorter.

With regards to the $C_1-S_5-O_8-C_9$ and $S_5-O_8-C_1-C_{10}$ dihedral angles, the differences between MP2/6-31G* and B3LYP/6-31G* amount to 4.1° and 7.5°, respectively. Similarly, they are very sensitive to the size of the basis set for the C_1 conformer. As reported in Table 2, these differences generally decrease when the size of the basis set is augmented. PBE1PBE and MPW1PW91 functionals yield results closer to those of MP2 than those of B3LYP for the $S_5-O_8-C_1-C_{10}$.

The B3LYP/6-311++G** calculation gave the lowest energy for the I (or III) and II conformers. The energy of the II conformer was always lower than that for the I and III conformers, regardless of the method and basis set used. Such a difference in energy amounts to 0.750 kcal/mol with ZPE correction. Both conformations (I and II) for $CH_3SO_2OCH_2CH_3$ are separated by a very low barrier arising from the rotation of ±159° (B3LYP/6-31G* calculation) around the SO bond. The prediction that the conformer having a symmetry plane is the most

TABLE 2: Geometry Parameters (bond distances in Å and bond angles in degrees) for the $CH_3SO_2OCH_2CH_3$ Molecule at Different Levels of Theory

	conformer II (C_s)						anion				conformer I (C_1)					
	6-31G*		B3LYP/	6-311++G**			6-311++G**				6-31G*		B3LYP/	6-311++G**		
	MP2	B3LYP	6-311G**	B3LYP	PBE1PBE	MPW1PW91	MP2/6-31G*	B3LYP	PBE1PBE	MPW1PW91	MP2	B3LYP	6-311G**	B3LYP	PBE1PBE	MPW1PW91
								Distances (Å)								
C1−H2,3,4	1.090	1.091	1.087	1.088	1.089	1.088	1.092	1.091	1.091	1.090	1.090	1.091	1.088	1.088	1.089	1.089
C1−S5	1.771	1.795	1.792	1.793	1.772	1.774	1.804	1.829	1.809	1.810	1.773	1.795	1.793	1.793	1.773	1.775
S═O	1.461	1.462	1.456	1.457	1.448	1.448	1.488	1.489	1.479	1.479	1.462	1.463	1.455	1.457	1.448	1.455
S−O	1.637	1.642	1.639	1.641	1.621	1.621	1.488	1.489	1.479	1.479	1.637	1.642	1.638	1.641	1.621	1.621
O−C	1.461	1.458	1.460	1.461	1.447	1.448					1.462	1.459	1.462	1.462	1.447	1.449
C−C	1.510	1.516	1.513	1.514	1.506	1.507					1.514	1.520	1.518	1.518	1.510	1.510
C9−H11, 12	1.094	1.095	1.093	1.093	1.094	1.095					1.092	1.093	1.090	1.090	1.092	1.091
C10−H13,14,15	1.092	1.095	1.092	1.092	1.093	1.091					1.093	1.095	1.092	1.092	1.093	1.091
O6···H11	3.46	3.50	3.50	3.50	3.46	3.46					4.29	4.31	4.32	4.33	4.29	4.30
O6···H12	2.73	2.76	2.79	2.79	2.74	2.75					3.73	3.63	3.66	3.75	3.75	3.75
O7···H11	2.73	2.76	2.79	2.79	2.74	2.75					3.82	3.82	3.82	3.83	3.81	3.81
O7···H12	3.46	3.50	3.50	3.50	3.46	3.46					2.44	2.47	2.48	2.47	2.45	2.45
								Angles (deg)								
H2−C1−H3,4	110.9	110.8	111.2	111.2	111.3	111.3	109.8	110.6	110.5	110.5	110.9	110.8	111.2	111.2	111.3	111.3
H2,3-C1−S5	108.8	108.8	108.5	108.4	108.6	108.6	109.1	108.4	108.4	108.5	108.9	108.9	108.58	108.6	108.7	108.7
H4−C1−S5	106.9	106.6	106.1	106.0	106.0	106.0	109.1	108.4	108.4	108.5	107.0	106.7	106.30	106.2	106.2	106.3
C1−S5−O6,O7	109.8	109.8	109.9	110.0	110.0	110.0	104.0	104.4	104.4	104.4	109.6	109.5	109.5	109.5	109.6	109.6
C1−S5−O8	96.2	96.3	96.5	96.7	96.9	96.9	104.0	104.4	104.4	104.4	96.6	96.5	96.75	97.3	97.5	97.5
O6−S5−O7	120.0	119.8	119.7	119.4	119.3	119.3	114.4	114.0	114.0	114.0	120.0	119.8	119.73	119.6	119.6	119.6
O6−S5−O8	109.2	109.3	109.2	109.2	109.1	109.1					109.9	110.0	109.79	109.7	109.6	109.6
O7−S5−O8	109.2	109.3	109.2	109.2	109.1	109.1					108.6	108.9	108.77	108.7	108.5	108.6
S5−O8−C9	113.6	115.0	116.1	116.3	115.5	115.8					115.4	116.8	117.87	118.2	117.6	117.8
O8−C9−C10	106.2	107.0	106.8	107.0	107.1	107.1					111.9	112.2	112.20	112.5	112.6	112.6
O8−C9−H11	108.5	108.5	108.5	108.4	108.4	108.4					102.7	103.2	103.04	102.8	103.1	103.0
O8−C9−H12	108.5	108.5	108.5	108.4	108.4	108.4					108.5	108.5	108.43	108.4	108.4	108.4
C10−C9−H11	112.1	111.8	111.8	111.8	111.8	111.8					111.8	111.6	111.63	111.6	111.6	111.6
H11−C9−H12	109.3	109.0	109.3	109.3	109.1	109.1					109.2	108.7	108.84	108.9	108.9	111.9
C9−C10−H13	109.6	109.5	109.5	109.4	110.4	109.4					110.3	109.4	109.31	109.1	110.5	108.9
H−C10−H	108.6	108.4	108.4	108.4	108.3	108.3					108.4	108.5	108.50	108.5	108.5	109.1
								Dihedral Angles (deg)								
C1−S5−O8−C9	180.0	180.0	180.0	180.0	180.0	180.0					−154.8	−158.9	−157.0	−152.8	−152.0	−151.6
S5−O8−C9−C10	180.0	180.0	180.0	180.0	180.0	180.0					−74.1	−81.0	−81.6	−78.6	−75.4	−76.1

TABLE 3: Energies without ZPE Correction for the $CH_3SO_2OCH_2CH_3$ and Anion at Different Levels of Theory (in Hartrees)

		conformer II (C_s)	anion	conformer I (C_1)
6-31G*	MP2	−741.3592608	−662.5064105	−741.3589806
	B3LYP	−742.9340426		−742.9334589
6-311G**	B3LYP	−743.0585434		−743.0577474
6-311++G**	B3LYP	−743.0671003	−663.9067501	−743.0661077
	PBE1PBE	−742.5263364	−663.4666344	−742.5256727
	MPW1PW91	−742.9782444	−663.8365210	−742.9774466

stable is unexpected in view of the conformations obtained through similar calculations made for the related molecules $CF_3SO_2OCH_3$,[5] $CF_3SO_2OSiH_3$,[6] $CF_3SO_2OSi(CH_3)_3$,[7] $CF_3SO_2OCH_2CF_3$,[8] $CCl_3SO_2OCH_2CF_3$,[9] and $CF_3SO_2OCH_2CH_3$.[10] In fact, in all cases the calculations predicted a *gauche* conformation with dihedral angles CSOC(Si) of 92−115° as the most stable structure, in agreement with the conformation measured and calculated for $CF_3SO_2OCH_3$,[5] which was considered a general structural property of covalent sulfonates. The C_s conformation for the EMS would favor nucleophilic attack when the alkylation of DNA occurs by an SN2 mechanism, which is very sensitive to steric hindrance, and is higher in the C_1 conformation than in the C_s. This fact, along with the properties of the mesylate leaving group, justifies its broad use as an ethylating agent in mutagenesis research.[1]

To gain some insight into the stability of these conformers, NBO calculations[4] were applied to the EMS compound. In the NBO analysis, the electronic wave function is interpreted as a set of occupied Lewis-type orbitals paired with a set of formally unoccupied non-Lewis-type orbitals. The electronic interactions within these orbitals, the deviations from the Lewis electronic structure, and the delocalization effects can be interpreted as a charge transfer between the filled Lewis orbitals (donors) and the theoretically empty non-Lewis orbitals (acceptors). The magnitude of these delocalization effects can be determined from an analysis of the off-diagonal elements in the Fock matrix in the NBO basis, taking into account all possible donor−acceptor interactions, and then calculating the stabilization energy associated to them by second-order perturbation theory. The stabilization achieved by each donation is measured through expression 1

$$\Delta E_{\sigma\sigma^*}^{(2)} = -2\frac{\langle\sigma|\hat{F}|\sigma^*\rangle^2}{\epsilon_{\sigma^*} - \epsilon_{\sigma}} \qquad (1)$$

$\Delta E_{\sigma\sigma^*}^{(2)}$ is the second-order energy lowering, σ and σ^* are, in a general sense, the donor and acceptor orbitals, respectively, and F is the Fock operator. It becomes apparent that two factors are conditioning the value $\Delta E_{\sigma\sigma^*}^{(2)}$: the energy gap between donor and acceptor orbitals and the off-diagonal element of the Fock matrix which, in turn, depends on the overlap between the involved orbitals.

Correspondingly, a NBO calculation was performed on EMS for both C_s and C_1 conformers at the B3LYP/6-311++G** level. After a careful analysis of the results, we found that the delocalization energy does not play a significant role in the relative stabilization of one conformer with respect to the other. The total contribution of $\Delta E_{\sigma\sigma^*}^{(2)}$ is 431.85 kcal mol^{-1} for the C_1 geometry and 431.78 kcal mol^{-1} for C_s, resulting in a difference of less than 0.1 kcal/mol. The main off-diagonal element in the Fock matrix is that corresponding to the energy transfer from the lone pair named LP(3)O_6 and LP(3)O_7 to the $\sigma^*S_5-O_8$. The magnitude of the interaction is 31.86 kcal/mol for the LP(3)$O_6 \rightarrow \sigma^*S_5-O_8$ and LP(3)$O_7 \rightarrow \sigma^*S_5-O_8$ for the C_s conformer and 32.07 kcal/mol for the LP(3)$O_6 \rightarrow \sigma^*S_5-O_8$ and 31.18 kcal/mol for the LP(3)$O_7 \rightarrow \sigma^*S_5-O_8$ for C_1. The occupancy and energy of the NBOs for both conformers are collected in Table 4.

TABLE 4: Energies and Occupancy of the Natural Bond Orbitals of $CH_3SO_2OCH_2CH_3$

	C_s		C_1	
	occupancy	energy (kcal/mol)	occupancy	energy (kcal/mol)
LP(3)O_6	1.77784	−0.30761	1.77414	−0.30554
LP(3)O_7	1.77784	−0.30761	1.78106	−0.31041
$\sigma^*S_5-O_8$	0.31395	0.06496	0.31608	0.06483
LP(2)O8	1.96511	−0.67997	1.96269	−0.66155
$\sigma_{C19-H11}$	1.98771	−0.53461	1.98754	−0.53385
$\sigma_{C19-H12}$	1.98771	−0.53461	1.97971	−0.53229
$\sigma^*_{C19-H11}$	0.02070	0.37997	0.01732	0.38279
$\sigma^*_{C19-H12}$	0.02070	0.37997	0.02054	0.38447

However, the main difference arises from an analysis of the localized σ bonding structure. The lone pair named LP(2) of O8 (in the molecular backbone) is considerably more stable in the C_s conformer than that in C_1. The same trend is observed for the σ_{C9-H11} and σ_{C9-H12} bond orbitals and their antibonding counterparts. The energies and occupancy of the NBOs are listed in Table 4. This relative stabilization of the C_s conformer could be interpreted through a repulsive interaction between the lone pair of the O_8 and the electronic charge of the bonds C_9-H_{11} and C_9-H_{12}, which is minimized when the symmetry is C_s.

For the mesylate anion, a local minimum of the potential energy surface is found for the conformer with C_{3v} symmetry, and a comparison of MP2 and DFT data yields very good agreement in the values of the molecular geometry parameters (see Table 2). As stated previously, our aim is to test the performance of that species as a leaving group in a nucleophilic substitution mechanism. Consequently, we have tested its capability to stabilize the excess of electronic charge following nucleophilic substitution by delocalization, using NBO analysis that provides an easy method to measure such a feature, bearing in mind the electron donation between donor−acceptor pairs of natural orbitals.

It should be noted that due to the symmetry of the system the three oxygen atoms of the SO_3 group, and their respective lone pairs, are equivalent. Hence, it is clear the excess of electronic charge of the mesylate anion is uniformly distributed among the three oxygen atoms. Furthermore, it becomes apparent from Table 5 that the lone pairs of the oxygen are donating electronic charge in the geminal σ^*(S−O) orbitals as well as in the vicinal σ^*(S2−C3). The important contribution of LP(3)O$y \rightarrow \sigma^*$(S2−C3) (where $y = 1$, 4, or 5) to the delocalization is driven by the polarization of the acceptor orbital toward the sulfur atom (54.94% on S, 45.06% on C) making a significant overlap possible with the donor LP(3)Oy orbitals. Also, the low energy gap between them, 0.39 kcal/mol, favors a high value of $\Delta E_{\sigma\sigma^*}^{(2)}$. Also the contribution of the sulfur atom to the stabilization of the excess of electronic charge through its Rydberg orbitals in transferences of the type LP(n)O1 → RY*S2 (where $n = 1$, 2, 3) is remarkable (see Table 5).

As mentioned in the Introduction, the carcinogenic and mutagenic potency of EMS has been studied some time ago

TABLE 5: Main Contributions to the Delocalization of the Excess of Electronic Charge in Mesylate Anion (energy units are kcal/mol)

donor → acceptor	$\Delta E_{\sigma\sigma^*}^{(2)}$	$\epsilon_{\sigma^*} - \epsilon_{\sigma}$	$\langle\sigma\|\hat{F}\|\sigma^*\rangle^2$
LP(1)O1 → σ*(S2−C3)	0.54	0.92	0.021
LP(1)O1 → σ*(S2−O4)	0.90	1.10	0.029
LP(1)O1 → σ*(S2−O5)	0.90	1.10	0.029
LP(2)O1 → σ*(S2−O4)	14.80	0.56	0.082
LP(2)O1 → σ*(S2−O5)	14.80	0.56	0.082
LP(3)O1 → σ*(S2−C3)	17.20	0.39	0.074
LP(3)O1 → σ*(S2−O4)	4.14	0.56	0.043
LP(3)O1 → σ*(S2−O5)	4.14	0.56	0.043
LP(1)O1 → RY(1)*S2	5.98	2.43	0.108
LP(2)O1 → RY(1)*S2	8.30	1.11	0.088
LP(3)O1 → RY(5)*S2	8.00	1.07	0.085

TABLE 6: O−C and S−O Bond Distances (Å) Calculated at the B3LYP/6-311++G Level for Different Molecular Systems (in angstroms)**

	$CH_3SO_2OCH_2CH_3$	$CH_3SO_2OCH_3$[a]
O−C	1.461	1.448
O−S	1.641	1.644

[a] Reference 11.

and also compared with other similar compounds, such as methyl methanesulfonate, $CH_3SO_2OCH_3$ (MMS)[1,3] as electrophiles inducing mutations by nucleophilic reactions. Therefore, it could be interesting to establish a correlation between those properties and the electronic structure optimized for EMS and MMS. Since for both cases the leaving group is the mesylate anion, the alkyl donor ability must depend, among other factors, on the strength of the R−X bond, where X = $CH_3SO_3^-$ and R = alkyl. In Table 6, the C−O bond distances calculated at the B3LYP/6-311++G** level in the case of EMS and MMS[11] for the most stable conformer, that is, C_s are listed. This is longer for EMS than for MMS, showing values of 1.461 and 1.448 Å, respectively, while the S−O bond distances are almost the same in both cases: 1.641 and 1.644 Å, respectively.

As a result, it may be expected that the mutagenic and/or carcinogenic potency would be higher for EMS than for MMS due to the higher ease with which the bond between the leaving group and the alkyl group can be broken. This behavior has been detected in some cases studied in ref 1, while in others, the trend is reversed because of other factors such as steric hindrance, solvent, etc. A comparative study of the influence in the SN1 and SN2 mechanisms of all these factors by using different alkyl groups (methyl, ethyl, and isopropyl) and/or leaving groups (mesylate, $MeSO_3^-$ and triflate, and $CF_3SO_3^-$) will be the subject of future works.

5. Vibrational Results

Assignment of the experimental bands to the normal modes of vibration of EMS was based on the comparison with related molecules[6−10,26−28] and with the results of the calculations performed here. The C_s conformer is 0.370 kcal/mol higher in energy using the B3LYP/6-31G* method than the C_1 conformer and at room temperature, where C_1 and C_s can be expected to be significantly populated. IR spectroscopy is an important auxiliary technique for quantitative conformational analysis.[29] However, a temperature variation study to find ΔH values from the van't Hoff equation is out of the scope of this work. The conformationally averaged IR spectrum was simulated by summing the population-weighted spectra of the C_s and C_1 conformers calculated by using B3LYP/6-31G* frequencies and intensities using Lorentzian band shapes (γ = 2 cm^{-1}). The populations were calculated from the B3LYP/6-31G* energy difference using Boltzmann statistics that amounted to 65% and 35%, respectively. This yielded a conformationally averaged IR spectrum that is much closer to that of C_s than to that of C_1 and leads straightforwardly to the assignment of the experimental spectrum shown in Figure 1.

At room temperature, most bands are attributable to the same fundamental for both conformations. The IR spectrum of the solid demonstrates the presence of C_s and C_1 geometries by the resolution of the fundamentals ν_{12}(A′), ν_{14}(A′), ν_{16} (A′), ν_{29} (A″), and ν_{32} (A″) whose profiles have been simulated in Figure 7. The predicted conformational splittings for those modes are generally in good agreement with the observed splittings in the IR spectrum of the solid. The vibrational analysis and force field have only been performed for the most stable conformer, C_s.

The B3LYP calculations reproduced the normal frequencies of $CH_3SO_2OCH_2CH_3$ with the following rmsd (root-mean-square deviation) for each basis set: 6-31G*, 78 cm^{-1}; 6-311G**, 61 cm^{-1}; 6-311++G**, 61 cm^{-1}. Although the second and third basis sets reproduce the experimental frequencies somewhat better, the results obtained with the combination B3LYP/6-31G* were used for the vibrational analysis, to facilitate comparison of the present results with those obtained previously for related molecules.[6−10,26−28] In fact, the combination B3LYP/6-31G* is being extensively used for vibrational calculations as a good compromise between economy of computational resources, accuracy, and applicability to many-atom systems. The frequencies calculated with this method for the 39 normal modes of vibration of $CH_3SO_2OCH_2CH_3$ (23 A′ + 16 A″) appear in Table 7 where they are compared with the measured values.

5.1 Assignment of Bands. 5.1.1. Methyl and Methylene Group Modes. Four strong, clearly defined bands and some shoulders appear in the IR and Raman spectra of the liquid substance in the complex 3080−2850 cm^{-1} region, and those features can be assigned to the expected eight CH stretching modes. The IR spectrum of the solid shows more features, and reference will be made to this spectrum below. The band located at 2939 cm^{-1} and the doublet at 3027−3031 cm^{-1} are assigned to the symmetric and antisymmetric stretching modes, respectively, of the methyl group bonded to S, with similar values to those observed in liquid CH_3SO_2OH,[26] that is, 2942 and 3029 cm^{-1}.

The previously reported spectra of $CF_3SO_2OCH_2CH_3$[10] were used as a guide for the assignment of other bands. The pair 2996−2981 cm^{-1} and the band at 2874 cm^{-1} are assigned to the antisymmetric and symmetric stretching modes of the methyl group in CCH_3, these being near the corresponding bands of the fluorinated molecule, at 2997 and 2887 cm^{-1}. The bands at 3013 and 2947 cm^{-1} are assigned to the CH_2 antisymmetric and symmetric stretching bands, respectively, which are also near to the corresponding bands in the fluorinated compound, at 3019 and 2950 cm^{-1}.

The CH_3 and CH_2 bending modes should appear in the 1300−1500 cm^{-1} region, which shows several bands and shoulders that are better defined in the spectra of the solid substance. The previously reported spectra of $CF_3SO_2OCH_2CH_3$[10] as well as the relative position of bands predicted by the calculations were used as arguments for the assignment of bands to these bending modes. The higher frequency band, located at 1482 cm^{-1}, is assigned to the CH_2 deformation, which appears at 1460 cm^{-1} (liquid spectrum) in the fluorinated compound. The calculations predict the methyl group deformation modes in CCH_3 to be at higher frequencies than in the SCH_3 moiety. Correspondingly,

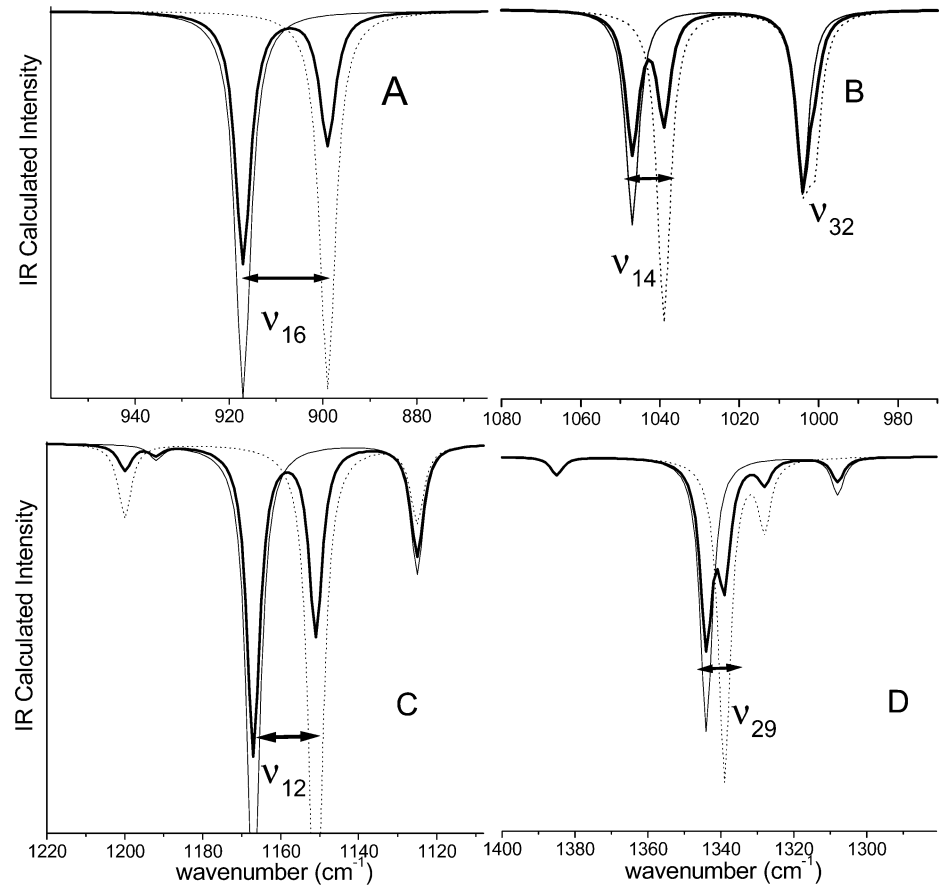

Figure 7. Calculated infrared spectra from B3LYP/6-31G* frequencies and intensities using Lorentzian band shapes: (A) region between 860 and 960 cm^{-1}, (B) region between 980 and 1080 cm^{-1}, (C) region between 1120 and 1220 cm^{-1}, and (D) region between 1300 and 1400 cm^{-1}. The bold solid line represents the conformationally averaged IR spectrum. The populations for both conformers C_s and C_1 are calculated from the B3LYP/6-31G* energy difference using Boltzmann statistics and are 65% and 35%, respectively. The normal solid line represents the IR spectrum for the C_s conformer, and the dotted line represents that for the C_1 conformer.

a shoulder at 1457 cm^{-1} and the band at 1450 cm^{-1} are assigned to the CH_3 antisymmetric deformation mode for CCH_3, whereas the symmetric deformation mode is expected to have a frequency about 100 cm^{-1} lower according to the calculations. The corresponding band is thus probably overlapped by the intense SO_2 stretching band. The pair of bands at 1411 and 1430 cm^{-1} would correspond to the CH_3 antisymmetric deformation modes in the SCH_3 group. The corresponding symmetric deformation mode is also predicted by the calculations at a frequency about 100 cm^{-1} lower, and therefore it probably corresponds to the band which appears at 1315 cm^{-1} in the low-frequency wing of the intense SO_2 stretching band in the spectrum of the solid substance. These modes appear at 1418 and 1336 cm^{-1} in the IR spectrum of liquid CH_3SO_2OH.[26] Taking into account the calculated difference in frequency between the CH_2 bend, CH_2 wagging, and CH_2 twisting modes, the bands located at 1482 (mentioned above), 1394, and 1281 cm^{-1} are assigned to these group vibrations.

The calculations show that the methyl rocking modes in the CCH_3 group are split by about 67 cm^{-1} and that they appear at higher frequencies than those for the SCH_3 moiety. The bands located at 1168 cm^{-1} (Raman) and 1103 cm^{-1} (liquid IR) are thus assigned to these nondegenerate modes. The bands that appear at 989 and 977 cm^{-1} in the spectrum of the solid are assigned to the same mode observed at 976 cm^{-1} in the liquid spectrum for the SCH_3 group. The experimental splitting is not predicted in Figure 7B. Finally, the 797 cm^{-1} band (liquid spectrum) is assigned to the CH_2 rocking mode located at 814 cm^{-1} in $CF_3SO_2OCH_2CH_3$.[10]

5.1.2. SO2 Group Modes. The SO_2 antisymmetric and symmetric stretching modes appear in the 1357−1467 and 1140−1200 cm^{-1} regions, respectively, in the CY_3SO_2X molecules reported previously.[6−10,26−28] Therefore, the bands observed at 1351 and 1175 cm^{-1} in the spectrum of the liquid are immediately assigned to these modes. These modes appear split in the IR spectrum of the solid as a doublet 1158/1169 cm^{-1} (see Figure 1) in the case of the mode observed at 1175 cm^{-1} in the liquid and at 1354/ 1328 cm^{-1} in the case of that observed at 1351 cm^{-1}. These splittings are in agreement with those calculated (see parts C and D of Figure 7) and may indicate the presence of both conformers in the solid IR spectrum.

The band at 530 cm^{-1} in the IR spectrum of the liquid is assigned to the SO_2 bending mode, which appears in the 488−538 cm^{-1} region in the above compounds. The three low-frequency modes corresponding to the movements of the whole SO_2 group will now be considered. The following assignments are proposed, with the corresponding assignment regions for the above molecules in parentheses: SO_2 wagging, 550 cm^{-1} (510−628 cm^{-1}); SO_2 rocking, 463 cm^{-1} (382−463 cm^{-1}); SO_2 twisting, 325 cm^{-1} (310−351 cm^{-1}). These assignments are also supported by the calculations.

5.1.3. Skeletal Modes. The CO stretching mode appears to be strongly mixed with CC stretching in these types of molecules. In fact, these vibrations are the main source of the 1009 cm^{-1} band, which can be described as the antisymmetric stretching of the CCO moiety in the molecular skeleton. CO stretching also appears as the main component of the intense

TABLE 7: Observed and Calculated Frequencies, Infrared and Raman Intensities, and Potential Energy Distribution for $CH_3SO_2OCH_2CH_3$

mode	observed	calculated [a]	calc. SQM[b]	IR intensities[c]	Raman activity[d]	potential energy distribution (≥10%)
				A′		
1	3027	3195	3028	0.09	69.12	100 S_1
2	2996	3135	3004	20.94	83.11	100 S_2
3	2947	3096	2945	0.01	103.00	99 S_3
4	2939	3074	2934	16.78	67.50	100 S_4
5	2875	3064	2872	14.16	122.40	100 S_5
6	1482	1551	1478	3.29	2.96	98 S_6 + 10 S_7
7	1457	1530	1463	2.62	21.56	13 S_6 + 74 S_7
8	1411	1488	1425	6.71	11.56	91 S_8
9	1394	1447	1406	10.93	6.82	79 S_9 + 12 S_{10} + 11 S_{14}
10	-	1415	1370	4.46	1.24	15 S_9 + 88 S_{10}
11	1315	1385	1324	12.81	0.65	100 S_{11}
12	1175	1167	1178	139.48	3.80	60 S_{12}
13	1103	1125	1118	38.13	10.19	24 S_{12} + 31 S_{13} + 16 S_{14} + 14 S_{21}
14	1009	1047	1021	88.08	3.00	31 S_{14} + 25 S_{15} + 30 S_{16}
15	989	1004	990	72.50	4.07	19 S_{14} + 43 S_{15} + 18 S_{16}
16	921	917	907	228.25	1.05	10 S_9 + 13 S_{13} + 11 S_{14} + 37 S_{16} + 28 S_{18}
17	816	775	807	87.99	6.09	60 S_{17} + 13 S_{19}
18	733	726	750	66.83	24.02	20 S_{13} + 56 S_{18} + 14 S_{21} + 14 S_{23}
19	550	525	558	30.09	8.11	20 S_{17} + 48 S_{19}
20	530	495	525	23.37	6.22	75 S_{20}
21	358	332	364	1.05	2.06	11 S_{18} + 21 S_{20} + 49 S_{21} + 46 S_{22}
22	338	304	329	6.37	3.60	11 S_{15} + 30 S_{19} + 32 S_{22} + 13 S_{23}
23	200	154	173	8.32	0.52	13 S_{21} + 41 S_{22} + 64 S_{23}
				A″		
24	3031	3206	3039	0.08	52.12	100 S_{24}
25	3013	3148	3006	29.80	17.03	50 S_{25} + 49 S_{26}
26	2981	3120	2984	2.50	78.84	50 S_{25} + 52 S_{26}
27	1450	1513	1445	6.28	19.82	92 S_{27}
28	1430	1482	1416	4.04	15.61	91 S_{28}
29	1351	1344	1347	192.84	3.44	91 S_{29}
30	1281	1308	1288	26.66	9.78	79 S_{30}
31	1168	1192	1161	4.17	2.15	28 S_{31} + 52 S_{33}
32	976	1003	967	0.92	6.44	78 S_{32}
33	797	831	814	0.87	0.14	17 S_{30} + 58 S_{31} + 48 S_{33}
34	463	443	470	12.48	1.68	72 S_{34} + 11 S_{35}
35	325	295	318	1.04	1.54	13 S_{32} + 22 S_{34} + 54 S_{35} + 32 S_{36}
36	287	246	291	0.03	0.21	35 S_{35} + 62 S_{36}
37	227	188	229	0.08	0.018	100 S_{37}
38	85	50	61	1.80	0.38	55 S_{38} + 37 S_{39}
39	-	34	44	3.69	0.15	55 S_{38} + 89 S_{39}
rmsd (cm^{-1})		78	9			

[a] B3LYP/ 6-31G* calculation. Observed and calculated values in cm^{-1}. [b] From scaled quantum mechanics force field (see text). [c] Units are km mol^{-1}. [d] Units are $Å^4/(amu)^{-1}$.

921 cm^{-1} band, strongly coupled with the SO stretching. The mode observed at 1009 cm^{-1} in the spectrum of the liquid appears as a peak at 1018 cm^{-1} and a shoulder at 1011 cm^{-1} in the IR spectrum of the solid. The second, at 921 cm^{-1} in the liquid, appears as a band at 940 cm^{-1} and a shoulder at 927 cm^{-1} in the solid. Both observations are in agreement with the calculations (see parts A and B of Figure 7).

The 816 cm^{-1} band is assigned to the C−S stretching, which has been reported at 748 and 770 cm^{-1} in monomeric[26] and dimeric CH_3SO_2OH,[26,28] respectively. The medium intensity band at 733 cm^{-1} in the IR spectrum of the liquid is assigned to S−O stretching on the basis of the calculated frequencies and comparison with $CCl_3SO_2OCH_2CF_3$[9] and $CF_3SO_2OCH_2CH_3$.[10]

No modes are predicted between 443 and 332 cm^{-1} and between 463 and 358 cm^{-1}. Eight modes are predicted by the calculations below 400 cm^{-1}. However, only six weak broad features appear below 400 cm^{-1} in the IR and Raman spectra of $CH_3SO_2OCH_2CH_3$, the 338 cm^{-1} band being the only well-defined feature in this region. These six bands were assigned taking into account the calculated frequencies and relative intensities.

According to the calculations, the poorly defined band at ca. 200 cm^{-1} in the Raman spectrum corresponds to a mode with the SOC bending coordinate as the main contribution. The shoulder at 358 cm^{-1} is assigned to OCC bending strongly mixed with CSO bending, this being similar to a mode at 359 cm^{-1} in $CF_3SO_2OCH_2CH_3$.[10] The CSO bending also contributes strongly to the 338 cm^{-1} mode.

5.1.4. Torsional Modes. The weak bands observed at 287 and 227 cm^{-1} are assigned to the CCH_3 and SCH_3 torsional modes. The broad 85 cm^{-1} feature is assigned to the torsion of the SO bond, with increased frequency because of the condensed state of the substance. These assignments are, however, only tentative due to the weakness and ill-defined nature of the bands.

5.2 Calculation of Force Constants. The force field in Cartesian coordinates, as generated by Gaussian code, was transformed to the set of nonredundant, natural coordinates defined in Table 1S (Supporting Information). Such coordinates take into account the local symmetry around the C, S, and O atoms and follow the proposals of Pulay et al.[12−15] The resulting force constants were scaled according to the methodology mentioned in Computational Details. A set of initial scale factors was defined using values recommended by Kalincsák and

TABLE 8: Scaling Factors for the Force Field of $CH_3SO_2OCH_2CH_3$

coordinates[a]	initial scale factor	final scale factor
ν SCH_3	0.920	0.899
ν CCH_3	0.920	0.908
ν CH_2	0.920	0.918
δ, ρ CH_3	1.000	0.912
ν C−O, ν C−C	0.922	0.933
ν SO_2	1.042	1.007
δ, wag, tw, ρ CH_2	1.000	0.970
δ, wag, tw, ρ SO_2	1.000	1.126
ν S−O	1.042	1.059
ν C−S	1.042	1.166
SCH_3, CCH_3 S−O, C−O, torsions	1.000	1.477
δ SOC, , δ OOC, δ CSO	1.196	1.274

[a] ν, stretching; δ, deformation; ρ, rocking; wag, wagging; tw, twisting.

TABLE 9: Force Constants in Internal (valence) Coordinates for $CH_3SO_2OCH_2CH_3$ and Related Molecules[a]

force constant	$CH_3SO_2OCH_2CH_3$[b] B3LYP/6-31G*	$CF_3SO_2OCH_2CH_3$[c] B3LYP/6-31G*	CH_3SO_2OH[b] B3LYP/6-31G*
f (C−H) (CH_2)	4.86	4.90	-
f (C−H) (CH_3)	4.96−4.82	4.84	4.91
f (C−S)	3.61	3.11	3.47
f (S−O)	4.15	5.04	4.31
f (S═O)	9.58	10.73	10.2
f (C−C)	4.36	4.27	
f (C−O)	4.18	4.20	
f (O═S═O)	1.28	1.14	1.35
f (O−S═O)	1.34	1.27	1.41
f (C−S−O)	1.48	1.13	1.31
f (C−S═O)	1.12	1.04	1.21
f (O−C−H)	0.72	0.69	
f (H−C−H)	0.50 (CH_2)	0.49	
f (H−C−H)	0.42−0.45 (CH_3)	0.46	0.42
f (S−C−H)	0.50		0.48

[a] Units are mdyn $Å^{-1}$ for stretchings and stretch/ stretch interactions and mdyn Å rad^{-2} for angular deformations. [b] This work. [c] Reference 10.

Pongor[15] in some cases and using the unity for the remainder, as shown in Table 8. These scale factors were subsequently refined by a nonlinear least squares procedure[9] in order to fit the 37 experimental frequencies.

The refined scale factors corresponding to each force constant appear in Table 8, whereas the resulting frequencies, rmsd final value, and potential energy distribution are supported in Table 7. It can be seen that only about one-half of the modes have a participation of ≥70% of a single coordinate, whereas other modes represent very complex vibrations in which several coordinates are involved.

The SQM force field (which is deposited as Supporting Information) was used to calculate the internal force constants appearing in Table 9, which are compared with the equivalent values of ethyl $CF_3SO_2OCH_2CH_3$[10] and CH_3SO_2OH, yielding good agreement. In the latter case, the force constant values were calculated using the same method and basis and with the experimental frequencies as ref 26.

6. Conclusions

The optimized molecular geometry and conformation for ethyl methanesulfonate have been calculated using MP2 and DFT techniques and different basis sets. The structural results show the C_s conformation to be the most stable. The methanesulfonate anion was also studied at the same levels of theory. NBO calculations have been performed in order to justify the preferred conformation in the case of EMS and the electron charge stabilization in the case of the anion. IR and Raman spectra were obtained for ethyl methanesulfonate, $CH_3SO_2OCH_2CH_3$, in which bands assignable to 37 out of the expected 39 normal modes of vibration were observed. The presence of both conformations was detected in the solid IR spectrum. It was possible to to scale the theoretical force field by taking the observed frequencies as a basis. The resulting SQM force field served to calculate the potential energy distribution, which revealed the physical nature of the molecular vibrations and the force constants in internal coordinates, which were similar to the values previously obtained for related chemical species.

Acknowledgment. The research grants provided by CONICET (Consejo Nacional de Investigaciones Científicas y Técnicas), ANPCyT (Agencia Nacional de Promoción Científica y Tecnológica), and UNLP (Universidad Nacional de La Plata) are gratefully acknowledged, as well as the financial help received from CIUNT (Consejo de Investigaciones de la Universidad Nacional de Tucumán). We thank Prof. Gordon Kearley for his kindly help.

Supporting Information Available: Tables presenting the definition of natural internal coordinates for $CH_3SO_2OCH_2CH_3$ and scaled *F* matrix internal coordinates. This material is available free of charge via the Internet at http://pubs.acs.org.

References and Notes

(1) Roberts, J. J.; Warwick, G. P. *Nature* **1957**, *179*, 1181. Loveless, A. *Nature* **1958**, *181*, 1212. Neuffer, M. G.; Sun, L.; Minocha, J. L.; Arnason, T. J. *Nature* **1962**, *196*, 499. Ficsor, G. *Science* **1963**, *139*, 1296. Kodym, A.; Tessman, I.; Singer, B.; Froese-Gertzen, E. E.; Konzak, C. F.; Foster, R.; Nilan, R. A. *Nature* **1963**, *198*, 447. Kaplan, R. W.; Beckmann, H.; Rueger, W. *Nature* **1963**, *199* (4896), 932. Poddar, R. K.; Kumar, S. *J. Mol. Biol.* **1964**, *9* (2), 352. Swann, P. F.; Magee, Peter N. *Nature* **1969**, *223* (5209), 947. Fraenkel-Conrat, H. *Biochemistry* **1974**, *13*, *3* (9), 1913. Todd P. A., Brouwer J., Glickman B. W. *Mutat. Res.* **1981**, *82* (2), 239. Boffa, L. C.; Bolonegsi, C.; Mariani, M. R. *Mutat. Res.* **1987**, *190* (2) 119. Fariss M. W.; Pascoe G. A.; Reed D. J. *Science* **1985**, *227* (4688), 751. Kasai, P. H. *J. Am. Chem. Soc.* **1991**, *113*, 3 (9), 3317. Afza, R. *Methods Mol. Biol.* **2003**, *236*, 189. Johansson, F.; Evans, J.; Thummel, C. S. *Genetics* **2003**, *165* (3), 1397. Allkvist, A.; Erixon, K.; Malmvarn, A.; Nilsson, R.; Bergman, A.; Helleday, T.; Jenssen, D. *Mutat. Res.* **2004**, *563* (1), 35. Umar-Tsafe, N.; Mohamed-Said, M. S.; Rosli, R.; Din, L. B.; Lai, L. C. *Mutat. Res.* **2004**, *562* (1−2), 91. Wulff, B. B. H.; Thomas, C. M.; Parniske, M.; Jones, J. D. G. *Genetics* **2004**, *167* (1), 459.

(2) Li, W. *J. Chromatogr., A* **2004**, *1046*, 297.

(3) Sega, G. A. *Mutat. Res.* **2004**, *134* (2−3), 113.

(4) Reed, A. E.; Curtiss, L. A.; Weinhold, F. *Chem. Rev.* **1988**, *88* (6), 899.

(5) Trautner F.; Ben Altabef A.; Fernández L. E.; Varetti E. L.; Oberhammer H. *Inorg. Chem.* **1999**, *38*, 3051.

(6) Fernández, L. E.; Ben Altabef, A.; Navarro, A.; Fernández Gómez, M.; Varetti, E. L. *Spectrochim. Acta* **2000**, *56A*, 1101.

(7) Fernández, L. E.; Ben Altabef, A.; Varetti, E. L. *J. Mol. Struct*. **2000**, *553*, 255.

(8) Tuttolomondo, M. E.; Fernández, L. E.; Navarro, A.; Varetti, E. L.; Ben Altabef, A. *Spectrochim. Acta* **2004**, *60A*, 611.

(9) Tuttolomondo, M. E.; Navarro, A.; Varetti, E. L.; Ben Altabef, A. *Spectrochim. Acta* **2005**, *61*, 1011.

(10) Tuttolomondo, M. E.; Navarro, A.; Varetti, E. L.; Ben, Altabef A. *J. Raman Spectrosc*. **2005**, *36*, in press.

(11) Tuttolomondo, M. E.; Navarro, A.; Varetti, E. L.; Ben Altabef, A. To be published.

(12) Pulay, P.; Fogarasi, G.; Pongor, G.; Boggs, J. E.; Vargha, A. *J. Am. Chem. Soc.* **1983**, *105*, 7037.

(13) Rauhut, G.; Pulay, P. *J. Phys. Chem.* **1995**, *99*, 3093.

(14) Rauhut, G.; Pulay, P. *J. Phys. Chem.* **1995**, *99* 14572.

(15) Kalincsák, F.; Pongor, G. *Spectrochim. Acta* A **2002**, *58*, 999.

(16) Becke A. D. *J. Chem. Phys*. **1993**, *98*, 5648.

(17) Lee, C.; Yang, W.; Parr, R. G. *Phys. Rev.* **1988**, *B37*, 785.

(18) Hehre, W. J.; Radom, L.; Scheleyer, P. v. R.; Pople, J. A. *Ab initio Molecular Orbital Theory*; Wiley: New York, 1986.

(19) Perdew, J. P.; Burke, K.; Ernzerhof, M. *Phys. Rev. Lett.* **1996**, *77*, 3865. Erratum: *Phys. Rev. Lett.* **1997**, *78*, 1396.

(20) Adamo, C.; Barone, V. *J. Chem. Phys.* **1998**, *108*, 664.

(21) Frisch, M. J.; Trucks, G. W.; Schlegel, H. B.; Scuseria, G. E.; Robb, M. A.; Cheeseman, J. R.; Zakrzewski, V. G.; Montgomery, J. A., Jr.; Stratmann, R. E.; Burant, J. C.; Dapprich, S.; Millam, J. M.; Daniels, A. D.; Kudin, K. N.; Strain, M. C.; Farkas, O.; Tomasi, J.; Barone, V.; Cossi, M.; Cammi, R.; Mennucci, B.; Pomelli, C.; Adamo, C.; Clifford, S.; Ochterski, J.; Petersson, G. A.; Ayala, P. Y.; Cui, Q.; Morokuma, K.; Malick, D. K.; Rabuck, A. D.; Raghavachari, K.; Foresman, J. B.; Cioslowski, J.; Ortiz, J. V.; Stefanov, B. B.; Liu, G.; Liashenko, A.; Piskorz, P.; Komaromi, I.; Gomperts, R.; Martin, R. L.; Fox, D. J.; Keith, T.; Al-Laham, M. A.; Peng, C. Y.; Nanayakkara, A.; Gonzalez, C.; Challacombe, M.; Gill, P. M. W.; Johnson, B. G.; Chen, W.; Wong, M. W.; Andres, J. L.; Head-Gordon, M.; Replogle, E. S.; Pople, J. A. *Gaussian 98*, revision A.7; Gaussian, Inc.: Pittsburgh, PA, 1998.

(22) Gledening, E. D.; Badenhoop, J. K.; Reed, A. D.; Carpenter, J. E.; Weinhold, F. F. Theoretical Chemistry Institute, University of Wisconsin, Madison, WI, 1996.

(23) Wilson, E. B.; Decius, J. C.; Cross, P. C. *Molecular Vibrations*; McGraw-Hill: New York, 1955.

(24) Collier, W. B. *Program FCARTP* (QCPE #631); Department of Chemistry, Oral Roberts University, Tulsa, OK, 1992.

(25) Nielsen, A. B.; Holder, A. J. *GaussView, User's Reference*; GAUSSIAN Inc.: Pittsburgh, PA, 1997−1998.

(26) Durig, J. R.; Zhou, L.; Schwartz, T.; Gounev, T. J. *J. Raman Spectrosc.* **2000**, *31* (3), 193.

(27) Fernández, L. E.; Ben Altabef, A.; Varetti, E. L. *J. Mol. Struct*. **2002**, *612*, 1.

(28) Mihalopoulos, N.; Barnes, I.; Becker, K. H. *Atmos. Environ*. **1992**, *26A*, 807.

(29) Herrebout, W. A.; van der Veken, B. J.; Wang, A.; Durig, J. R. *J. Phys. Chem*. **1995**, *99*, 578.